Extrusion of Linear Polypropylene–Clay Nanocomposite Foams

Amit Kumar Chaudhary, Krishnamurthy Jayaraman
Department of Chemical Engineering and Materials Science, Michigan State University, East Lansing, Michigan 48824-1226

This work presents new results on using organoclay with an appropriate polymeric compatibilizer as rheology-modifying additives for extrusion foaming of a linear polypropylene (PP), which by itself does not display strain hardening in extensional flow of the melt. The uniaxial melt-extensional viscosity behavior of several nanocomposites prepared with varying ratio of bound maleic anhydride to clay as well as varying compatibilizer molecular weight was investigated. A chemical-blowing agent was used at a fixed concentration for foaming these nanocomposites in a single-screw extruder. Among nanocomposites with similar levels of clay dispersion or intercalation, the ones that displayed significant strain hardening in the melt state along with slower crystallization led to extruded PP nanocomposite foams with smaller cell sizes and greater cell density by reducing cell coalescence. This was achieved with as little as 3 wt% organoclay and a high-molecular weight PP-*g*-MA compatibilizer in linear PP. POLYM. ENG. SCI., 51:1749–1756, 2011. © 2011 Society of Plastics Engineers

INTRODUCTION

A variety of thermoplastic polymer foams with good cell structure have been produced from polystyrene [1, 2], polycarbonate [3], poly(lactic acid) [4], and poly(ethylene terephthalate) [5]. However, the production of closed-cell foams with linear polypropylene (PP) is difficult, because it does not exhibit strain hardening under extensional flow [6, 7]. Polymer melts that do not exhibit strain hardening develop thinner cell walls during bubble expansion in the foaming process, which results in coalescence of bubbles and even open-cell foams [8–11]. The semicrystalline nature of PP also makes the foaming process more complicated because of simultaneous nucleation and growth of gas bubbles and crystals. Reignier et al. [12] have demonstrated with batch foaming of poly(ε-caprolactone) that crystallization affects both bubble nucleation and growth.

Correspondence to: K. Jayaraman; e-mail: jayarama@egr.msu.edu
DOI 10.1002/pen.21961
Published online in Wiley Online Library (wileyonlinelibrary.com).

It is well established that blends of linear PP and branched PP foam better than the linear resin [6, 13, 14], leading to more uniform cell sizes and higher cell densities than with the linear resin. This is because an increase in the extensional viscosity of the blends during the bubble expansion process provides stability to the cell walls [15–18]. These blends typically have 20 wt% of the branched polymer, which adds to the cost significantly. Partial crosslinking also leads to strain hardening in melt-extensional flow of PP [19–21] and results in better foam; however, the crosslinking process leads to loss of recyclability, chain scission, and oxidative degradation of the PP, which affect its physical properties [22, 23].

Striking improvements in polymer foam-cell structure upon adding organoclay have been demonstrated with the amorphous polystyrene by Lee and coworkers [1, 24], and these improvements have been attributed to the large number of nucleation sites provided by the clay surface. They reported over 50% reduction in average cell size and around 6–10-fold increase in cell densities of polystyrene nanocomposite foam by the addition of 5wt% organically modified clay. Other workers have applied this approach to the semicrystalline PP with only limited improvement in foam quality [25–28]. For example, Guo et al. [25] observed a 25% drop in average cell size of linear PP foam upon addition of organoclay. Gendron et al. [28] observed that addition of 2wt% of organoclay to the linear PP matrix produced only a slight improvement in the cellular structure of the foam samples. This may be attributed to the absence of extensional strain hardening in their linear PP clay nanocomposite melts. Strain hardening in uniaxial extensional flow of polymer–clay nanocomposite melts with a high-molecular weight maleated PP alone as the matrix has been reported by Okamoto et al. [29] and by Pathak and Jayaraman [30] with different organoclays. There is clearly a need for preparing and foaming nanocomposites that display significant strain hardening in extensional flow with linear PP as the matrix.

The objective of the present work was to investigate differences in foam quality produced from two sets of PP clay nanocomposites, all prepared with good dispersion of clay—one set that does not exhibit strain hardening in the

melt and another that does. These nanocomposites were prepared by using different ratios of compatibilizer to clay and two different grades of the compatibilizer. The foams were produced in a single-screw extruder with the same proportion of a chemical-blowing agent in all cases. It is worth noting here that the literature on foaming polymer nanocomposites has been focused largely on physical blowing. The results presented in this work show that besides providing a greater concentration of nucleating sites for foaming the polymer matrix, addition of organoclay with appropriate compatibilizer in the right proportions can provide favorable rheology modifications and also alter the crystallization kinetics favorably for extrusion of closed-cell PP foams.

EXPERIMENTAL

Materials

Linear PP (Profax 6523, 4 dg/min MFI; ASTM 1238) used in this study was supplied by Basell. Two grades of maleic anhydride-grafted PP (PP-g-MA) were used as compatibilizer in this study: Exxelor PO-1015 from ExxonMobil Chemical Co., labeled PP-*g*-MA1 here is a random copolymer with ethylene (M_w = 180,000; 0.5 wt% bound maleic anhydride) and AC-950 from Honeywell, labeled PP-*g*-MA2 here is a homopolymer (M_w = 22,000; 4 wt% maleic anhydride total and 2.6 wt% bound maleic anhydride). The nanoclay used in this study was organically modified montmorillonite clay, I.44P, supplied by Nanocor. The chemical-blowing agent used in this study was Cell-span 693K (gas volume 70 cc/g), provided by Phoenix Plastics with the active ingredient being azodicarbonamide.

Preparation of Nanocomposites

Five different PP–clay nanocomposites were compounded for this study. The details of the composition are provided in Table 1. Before compounding, the PP-*g*-MA and nanoclay were dried overnight at 80°C and 508 mm Hg vacuum in a vacuum oven. Dry nanoclay powder was premixed with PP resin and PP-*g*-MA in a bag and then melt compounded in a 47-g Banbury batch mixer at 180°C and at a rotation speed of 150 rpm for 10 min; this was done under a nitrogen blanket to avoid thermal degradation. The compounded material was then granulated in a mini granulator.

Extrusion of Foams

Continuous extrusion foaming with a chemical-blowing agent (Cell-span 693K) was used to prepare PP nanocomposite foams. In all the foaming runs, 3 wt% of the chemical-blowing agent was premixed with the granulated polymer compound in a bag and loaded into the hopper of a [3/4]" single-screw extruder, which was operated at 20 rpm. A 2-mm diameter die (L/D = 15), was mounted on this extruder with a tapered transition from the extruder barrel. The chemical-blowing agent and the PP nanocomposite fused to form a homogeneous melt in the extruder barrel. The three temperature zones in the extruder barrel were maintained at 180°C, 200°C, and 170°C in the order of distance from the hopper for all foaming experiments. The die temperature was maintained at 35°C above the crystallization temperature of the compound determined independently from DSC runs; this was found to be optimal here, as it helped to maintain a pressure drop of around 4000 psi with various polymer compounds. This is consistent with the work of Park et al. [31–33] and Naguib et al. [34] who report that the die temperature is critical for extrusion foaming: early onset of crystallization at lower temperatures leads to insufficient foaming while delayed onset of crystallization at higher temperatures causes foam collapse by gas diffusion.

TABLE 1. Composition of PP-clay nanocomposites.

Specimen	PP (wt%)	PP-*g*-MA (wt%)		Organoclay (wt%)	g-Mol bound MA/kg organoclay
		PP-*g*-MA1	PP-*g*-MA2		
PPNC-N2	68.0	—	24	8	0.80
PPNC-N1	68.0	24	—	8	0.15
PPNC-S1	40.0	52.8	—	7.2	0.37
PPNC-S2	76.0	21.0	—	3.0	0.35
PPNC-S6	85.0	12.0	—	3.0	0.20

Characterization

The dispersion of nanoclay in the PP matrix was characterized by X-ray diffraction (XRD) studies using a Rigaku Rotaflex Ru-200BH X-ray diffractometer, which is equipped with a Ni-filtered Cu Kα radiation source. The PP nanocomposite was molded in a compression molder at 180°C and 10 tons (20,000 pounds) into a 1-mm thick disc, 50 mm in diameter; a strip measuring 40 mm × 20 mm × 1 mm was cut out of this disc and used in the XRD studies. The sample is scanned over a 2θ range of 0.5–10° at a rate of 0.5°/min, and measurements are recorded at equal increments of 0.01°. The crystallization temperatures and crystallization rate of the nanocomposites were estimated by differential scanning calorimetry (TA Q-Series, DSC Q10). The sample (10 mg) was heated to 200°C (at 5°C/min ramp), then cooled to 40°C (−5°C/min ramp) under nitrogen atmosphere, and this was repeated; results are reported from the second run.

The melt-extensional viscosity was measured using an extensional viscosity fixture on a TA-ARES instrument. Test specimens (18 mm × 10 mm × 0.75 mm) were compression molded at 180°C and a pressure of 5 tons (10,000 pounds). The extensional viscosity measurements were made for the nanocomposites at 180°C and at four strain rates (0.1, 0.5, 1.0, and 2.0 s^{-1}) over Hencky strains up to 3. The densities of the foam samples were

 DOI 10.1002/pen

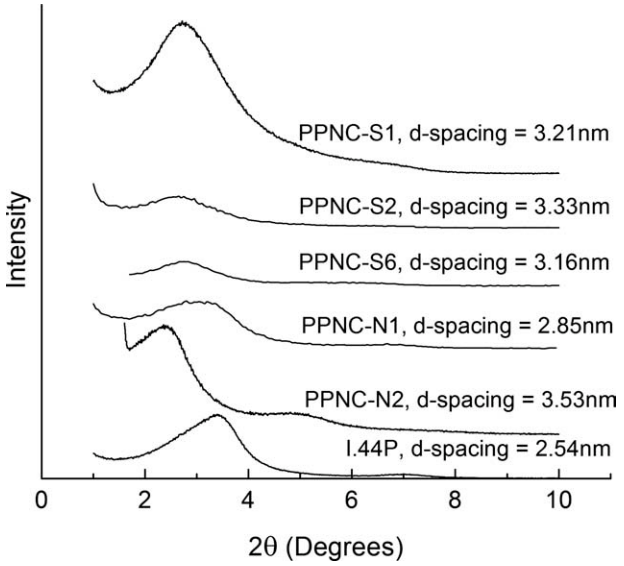

FIG. 1. X-ray diffraction patterns of the organoclay and the nanocomposites.

measured by the Archimedes water-displacement method (ASTM D792). The reported value of density is an average of 10 data points. The foam structure was studied by scanning electron microscopy (JEOL 6400). Foamed extrudates were cryogenically fractured, and the fractured surface was coated with osmium. SEM micrographs were taken from these fractured surfaces at a magnification of 60×. The average cell size, cell-size distribution, and cell density were evaluated using ImageJ software. The cell density was calculated with the following equation:

$$N = (n/A)^{3/2} \tag{1}$$

where n is the number of cell projections in the defined image area A, derived from SEM micrographs.

RESULTS AND DISCUSSION

Nanocomposite Structure

XRD patterns obtained for all the PP nanocomposites and for the nanoclay in the range of $2\theta = 1°–10°$ have been presented in Fig. 1. The mean interlayer spacing of the [001] plane (d-spacing) for the nanoclay used in this study was found to be 2.54 nm ($2\theta = 3.48°$). The d-spacing of the [001] plane was found to be higher in all the PP nanocomposites here, confirming intercalation by polymer. A comparison between PPNC-N1 and PPNC-N2 indicates a larger d-spacing of 3.53 nm in PPNC-N2, than in PPNC-N1 (2.85 nm). The higher maleic anhydride content in PP-*g*-MA2 (2.6 wt% bound maleic anhydride) compared to PP-*g*-MA1 (0.5 wt% bound maleic anhydride) allows greater hydrophilic interaction between the polar montmorillonite surface and the maleic anhydride groups of the polymer chains and results in greater intercalation of the polymer chains within the clay galleries. A comparison between PPNC-N1 and PPNC-S1 nanocomposites, which have similar clay loadings and different proportions of the same compatibilizer (PP-*g*-MA1), shows an increase in d-spacing with an increase in the proportion of compatibilizer, thus indicating that similar extents of nanolayer intercalation were achieved by increasing the weight fraction of the lower maleic anhydride content compatibilizer. Increasing the proportion of this compatibilizer above 4 provided very little change in the extent of intercalation as seen by comparing PPNC-S1, PPNC-S2, and PPNC-S6.

Extensional Viscosity

Although gas expansion within foaming polymers creates biaxial extensional flow in the melt, uniaxial extensional flow measurements are relevant, because measurements of biaxial extensional viscosity in lubricated squeezing tests display trends that are similar to trends in measurements of uniaxial extensional viscosity; cf. Munstedt et al. [12, 35]. In particular, they conclude that if strain hardening is observed in uniaxial extensional flow, it will be observed in biaxial extensional flow as well. This is useful, because more reliable equipment and procedures are available for the measurement of uniaxial extensional viscosity of melts than for the measurement of biaxial extensional viscosity of polymer melts.

The melt-extensional viscosity transients for the linear PP, PPNC-N1, and PPNC-N2 melts at 180°C and several strain rates have been presented in Fig. 2. The transients for the remaining nanocomposite melts have been presented in Fig. 3. For all specimens, as expected, the transient extensional viscosity curves measured at different strain rates superimpose at low strains to give the linear viscoelastic limit. Strain hardening of the melt is defined as an upward deviation of the extensional viscosity from this linear visco-

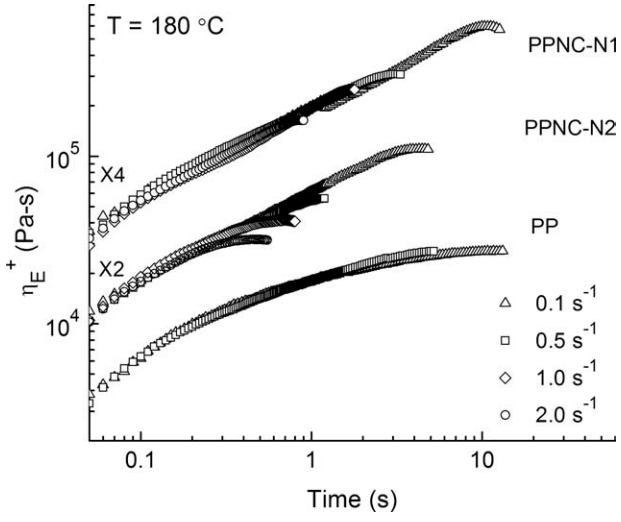

FIG. 2. Uniaxial extensional viscosity transients at 180°C of linear PP and nanocomposites PPNC-N1 and PPNC-N2.

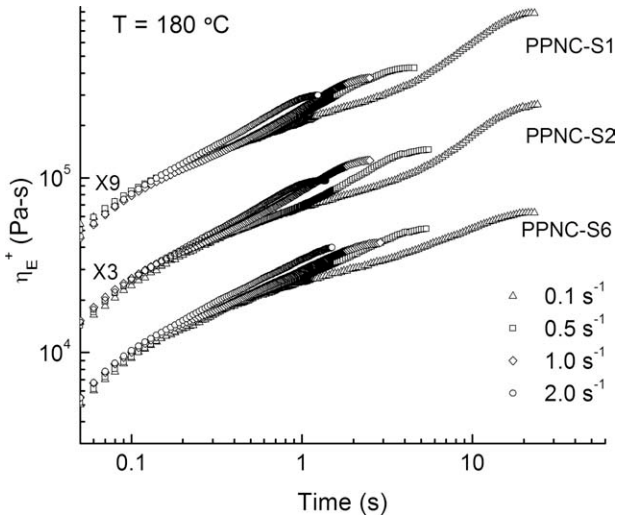

FIG. 3. Uniaxial extensional viscosity transients at 180°C of PPNC-S1, PPNC-S2, and PPNC-S6 nanocomposite melts.

elastic envelope usually at strains greater than one. The strain hardening parameter χ is defined as follows.

$$\chi = \frac{\eta_E^+(t,\dot{\varepsilon})}{\eta_{E0}^+(t)} \tag{2}$$

where $\eta_E^+(t,\dot{\varepsilon})$ is the transient extensional viscosity as a function of time and strain rate, and η_{E0}+(t) is the transient extensional viscosity in the linear viscoelastic regime. The linear viscoelastic η_{E0}+(t) may be determined in one of two ways: (a) as three times the transient shear viscosity growth curve at very low strain rates or (b) by extrapolating the superimposed portion of the curves for different strain rates. The two methods give the same result for homogeneous melts but may give different results for filled polymer systems and polymer–clay nanocomposites in particular because of differences in orientation of anisotropic filler particles in elongational and shear flows [29, 36]; hence method (b) was used for this work.

The transient extensional viscosity data for the linear PP melt did not show strain hardening. The extensional viscosity data for molten PP-*g*-MA compatibilizer did not show any strain hardening either. Amongst the PP nanocomposite melts, PPNC-N1 and PPNC-N2 showed no strain-hardening behavior. However, the transient extensional viscosity curves for PPNC-S1, PPNC-S2, and PPNC-S6 show significant strain hardening of the polymer melt at all strain rates tested. The strain-hardening parameter, estimated at a Hencky strain of 2.25, is plotted against strain rate for three strain-hardening melts at 180°C in Fig. 4; these curves shows that strain hardening in PPNC-S1, PPNC-S2, and PPNC-S6 melts decreased with increasing strain rate similar to the trend shown by blends of linear PP with up to 20 wt% of branched PP [14] as well as blends of linear PP with small amounts of crosslinked polymer [37]. The melts of PPNC-S1, PPNC-S2, and PPNC-S6 displayed similar strain-hardening behavior indicating that 3 wt% of organoclay and a 4:1 (wt) ratio of PP-*g*-MA to organoclay were adequate for producing this effect in linear PP/organoclay nanocomposites. The latter amounted to 0.2-g-mol bound maleic anhydride on the compatibilizer chains per kilogram organoclay as presented in Table 1, which represents one requirement for forming sufficient physical junctions (presumably by hydrogen bonding) between the hydroxyl groups at the organoclay edges and the compatibilizer chains, which may also form bridges between clay particles.

The other requirement arises from the density of trapped entanglements along the bridging compatibilizer chains. This may be seen from the fact that when the lower molecular weight compatibilizer was used with 0.8-g-mol bound maleic anhydride per kilogram organoclay, the resulting nanocomposite melt did not display strain hardening. Hence, strain hardening in the nanocomposite melts is analogous to that reported for blends containing small amounts of crosslinked polymer. Just as blends of linear PP with small amounts of chemically crosslinked polymers contain trapped entanglements on chain segments between crosslinks or junctions, which respond to stretching differently from entanglements and chain segments in the bulk [37], interactions between the surface or edge of the nanolayer and the maleated polymer can form a network of physical junctions or anchor points between which bridging compatibilizer chains trap entanglements to produce a similar effect. Thus, in addition to good dispersion and sufficient interaction between the compatibilizer and the clay surface or edge, the molecular weight of the compatibilizer should be high enough so as to form a sufficient number of trapped entanglements along the compatibilizer chain between clay surfaces or edges.

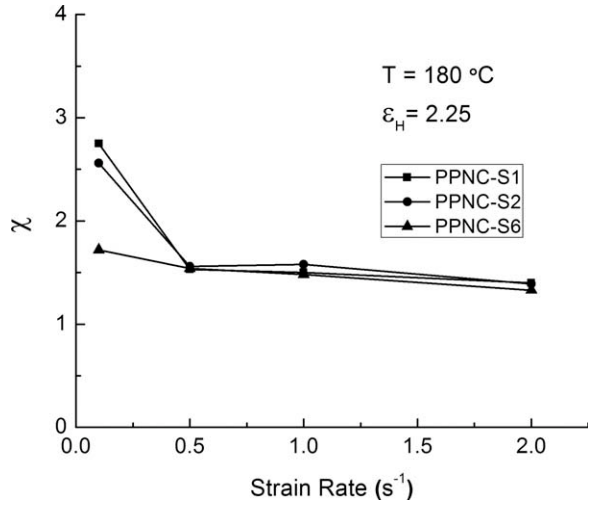

FIG. 4. Strain-hardening parameter at a Hencky strain of 2.25 versus strain rate for PPNC-S1, PPNC-S2, and PPNC-S6 nanocomposite melts at 180°C.

 DOI 10.1002/pen

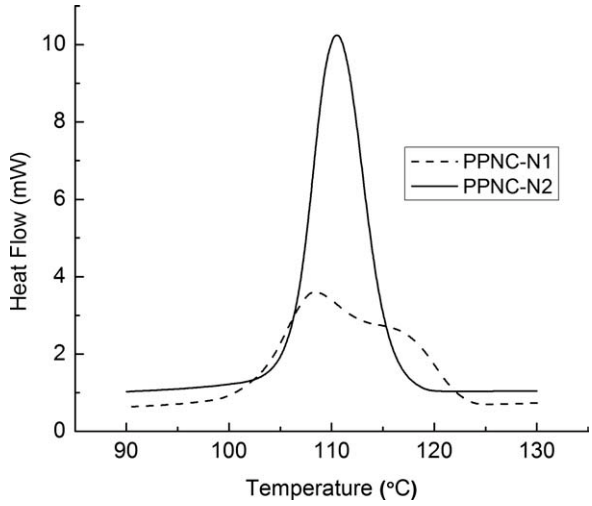

FIG. 5. Crystallization curves of nanocomposites PPNC-N1 and PPNC-N2.

Crystallization

Average rates of crystallization may be computed from the crystallization curves obtained with DSC tests for various nanocomposites. Crystallization curves have been presented for PPNC-N1 and PPNC-N2 in Fig. 5, and the crystallization curves for the remaining nanocomposites have been plotted in Fig. 6 along with the curve for PPNC-N2 as the base case. The cooling rate for all the DSC tests was 5°C/min. The fractional crystallinity (X_c) and the average rate of crystallization (k) in each sample were obtained by the following relations.

$$X_c = \frac{\Delta H_c}{207w}, \quad k = \frac{X_c}{t_c} \tag{3}$$

where w is the weight fraction of polymer in the sample, ΔH_c is the enthalpy of crystallization of polymer in the sample obtained by computing the area under the crystallization peak, the quantity 207 J/g refers to the enthalpy of crystallization of 100% crystalline PP, and t_C refers to the time span over which crystallization is completed. These results are tabulated in Table 2.

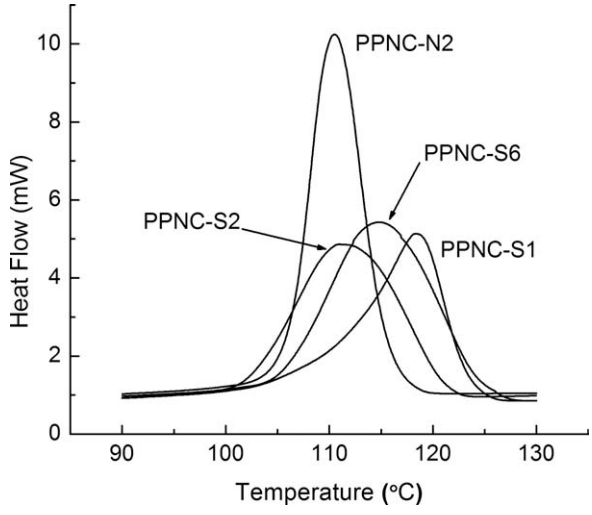

FIG. 6. Crystallization curves of PPNC-S1, PPNC-S2, and PPNC-S6 compared to the base case of PPNC-N2.

TABLE 2. Crystallinity and average rates of crystallization for PP and PP nanocomposites.

Specimen	Fractional crystallinity (X_c)	Time span t_c (min)	Average rate of crystallization (min^{-1})
PP	0.44	2.9	0.15
PP-*g*-MA1	0.34	3.9	0.09
PPNC-N1	0.35	5.0	0.07
PPNC-S1	0.36	5.1	0.07
PPNC-S2	0.38	5.0	0.07
PPNC-S6	0.39	5.1	0.08
PP-*g*-MA2	0.36	2.7	0.13
PPNC-N2	0.44	3.4	0.13

It is clear from Table 2 that both compatibilizers crystallized more slowly than the linear PP; this is consistent with the literature [38]. PP-*g*-MA1, being a random copolymer, displayed a lower rate of crystallization from the melt than PP-*g*-MA2, which is a hompolymer. Amongst the four nanocomposites studied in this work, PPNC-N2 has the highest rate of crystallization. The average rates of crystallization for PPNC-N1, PPNC-S1, PPNC-S2, and PPNC-S6 (each containing PP-*g*-MA1) were all about half of the rate for PPNC-N2 (which contains PP-*g*-MA2). This may be traced to the fact that PP-*g*-MA1 crystallized at about half the rate of PP-*g*-MA2.

Extruded Foam Structure

It is evident from the preceding sections that addition of nanoclay and a suitable compatibilizer to linear PP has the potential to produce three different effects: (a) greater surface area for nucleation of voids, (b) changes in crystallization rate of the PP, and (c) strain hardening in the melt state. PPNCs resulting in first two effects are commonly observed due to the addition of nanoclays and PP-*g*-MA, respectively; however, compounds composed of nanoclay and compatibilizer with linear PP and displaying strain-hardening behavior in extensional flow have not been reported previously. The absence or ordering of the three effects among the five different PP nanocomposites of this work has been summarized in Table 3. Extruded foam samples were inspected visually to determine whether they were open-cell or closed-cell foams. The foamed linear PP without any nanoclay particles turned out to be open-cell foam with very large cell sizes. Some open-cell structure was seen in PPNC-N2 foam as well. The rest of the nanocomposite foams were all closed-cell foams. The bulk densities for the various extruded foam samples are listed in Table 4 along with average cell sizes and cell number densities. The bulk density of foamed PPNC-N2 was close to the bulk density of the foamed linear PP matrix although the latter was open-cell foam. The bulk density of foamed PPNC-N1 was lower at 0.37, and each of the remaining nanocomposites—PPNC-S1,

TABLE 3. Comparison of polypropylene–clay nanocomposite characteristics.

Polymer	Surface area	Average rate of crystallization	Melt strain hardening
PPNC-N2	BASE	CASE	
PPNC-N1	=	_	=(None)
PPNC-S1	=	_	+
PPNC-S2	_	_	+
PPNC-S6	_	_	+

(−), lower than base case; (+), higher than base case; (=), same as base case.

TABLE 4. Characteristics of extruded foams from polypropylene and PP–clay nanocomposites.

Polymer	Foam density (g/cm^3)	Average cell size (μm)	Average cell density (no./cm^3)
Linear PP	0.4	—	—
PPNC-N2	0.4	170.9	0.1×10^6
PPNC-N1	0.37	132.7	0.6×10^6
PPNC-S1	0.3	86.5	1.3×10^6
PPNC-S2	0.3	87.0	1.2×10^6
PPNC-S6	0.3	87.9	1.2×10^6

PPNC-S2, and PPNC-S6 had a bulk density of 0.3 g/cc indicating similar levels of expansion.

The scanning electron micrographs for all the extruded foam samples are presented in Fig. 7. The scanning electron micrograph of a linear PP foam sample (Fig. 7a) shows evidence of severe cell coalescence and large scale inhomogeneity with regions of very low cell density. The micrograph of PPNC-N2 foam presented in Fig. 7b shows some improvement in quality with mostly closed-cell structure; however, most of the cells are larger than 200 μm. The improvement in cellular structure may be attributed to the increased surface area for heterogeneous nucleation in PPNC-N2 over the neat linear PP. Recall that neither PPNC-N1 nor PPNC-N2 showed melt strain hardening in extensional flow and both have the same level of nanoclay, but PPNC-N1 crystallizes slower than PPNC-N2. Hence a comparison between PPNC-N1 foam and PPNC-N2 foam would establish the effect of slower crystallization on foam characteristics. It is evident from comparing the SEM micrographs in Fig. 7b and c that PPNC-N1 foam has better cellular structure than PPNC-N2 foam. This is also evident from the cell-size distributions presented in Fig. 8 for the two nanocomposite foams. The cell density for PPNC-N1 foam was sixfold greater than that of PPNC-N2 foam, and the average cell size in PPNC-N1 foam was significantly lower as well. A lower rate of crystallization of the polymer matrix in PPNC-N1 led to a greater rate of bubble nucleation in the melt and also cut down the coalescence of bubbles. Still, PPNC-N1 foam had a lot of larger-sized cells (>200 μm) and a broad cell-size distribution.

Next, the effect of strain hardening in melt extensional flow on foam quality may be seen by comparing the cell-size distribution presented in Fig. 9 for the foam extruded from PPNC-S1 against that of the foam extruded from PPNC-N1. It is clear from Table 4 that PPNC-S1 resulted in foam with smaller average cell size and higher cell density. The cell-size distribution presented for PPNC-S1 is distinctly narrower with most cells in the range of 40–100 μm. Since the clay loading in PPNC-S1, the average rate of crystallization, the amount of blowing agent used, and the pressure drop during foaming were all very similar to that in PPNC-N1, and the improvement in foam quality with PPNC-S1 can be attributed to the strain hardening of the polymer melt in extensional flow. The enhanced strain-hardening behavior of the PPNC-S1 melt stabilizes the cell walls

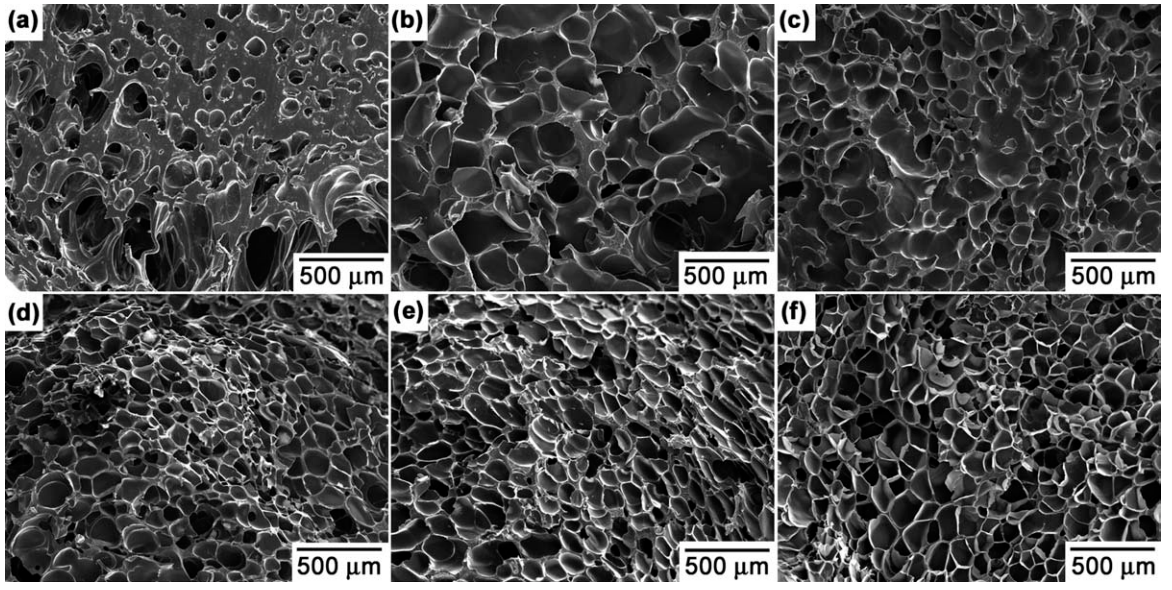

FIG. 7. Scanning electron micrographs of extruded foam samples for (a) linear PP foam, (b) PPNCN2 foam, (c) PPNC-N1 foam, (d) PPNC-S1 foam, (e) PPNC-S2 foam, and (f) PPNC-S6 foam.

 DOI 10.1002/pen

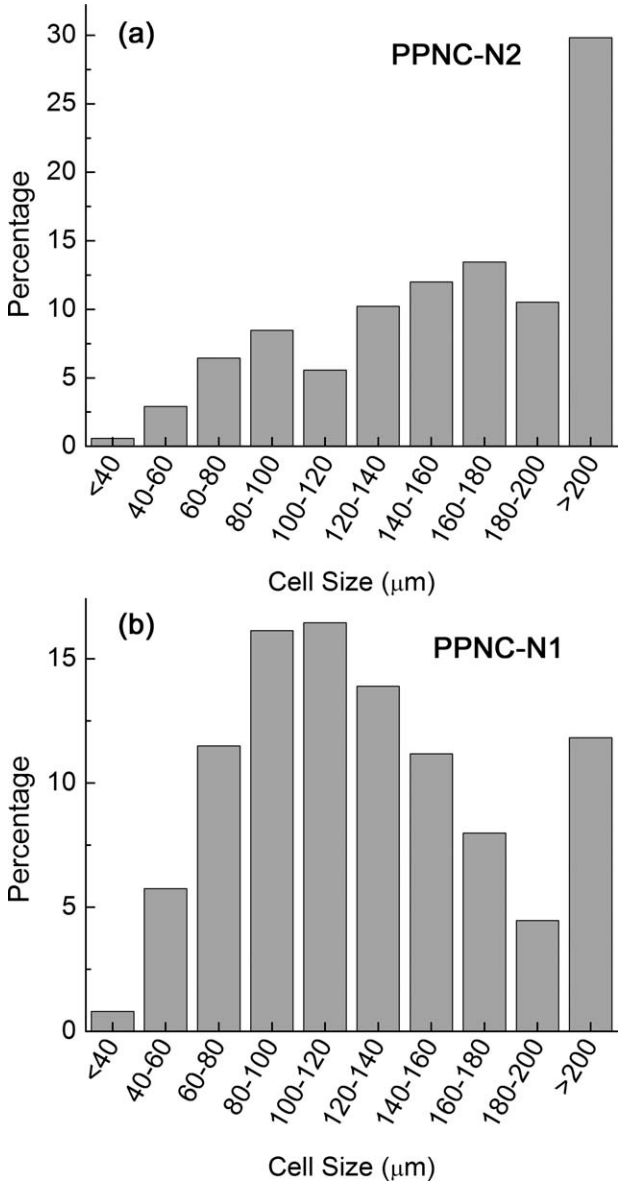

FIG. 8. Cell size distributions in extruded samples of (a) PPNC-N2 foam and (b) PPNC-N1 foam.

and limits coalescence. The absence of strain hardening in PPNC-N1 resulted in cell coalescence and led to larger cells.

Finally, the cell structures of foams produced with the three strain hardening compounds PPNC-S1, PPNC-S2, and PPNC-S6 may be compared. The three nanocomposites differ only in the amounts of organoclay and compatibilizer; all three show significant strain hardening under uniaxial melt extensional flow and have similar crystallization rates. From the SEM micrographs in Fig. 7d–f and the results in Table 4, it is evident that the three extruded foams have similar average cell sizes and cell densities. The cell-size distributions presented in Fig. 9 for PPNC-S1, PPNC-S2, and PPNC-S6 nanocomposite foams are also very similar. This indicates that high quality foams can be produced with only 3 wt% of nanoclay and a ratio of 0.2-g-mol maleic anhydride per kg of clay (see Table 1) in a compatibilizer with high molecular weight.

Results presented in this work on foams extruded from PP–clay nanocomposites with a chemical-blowing agent show progressive improvement in the quality of foam samples as one or more of the following features were

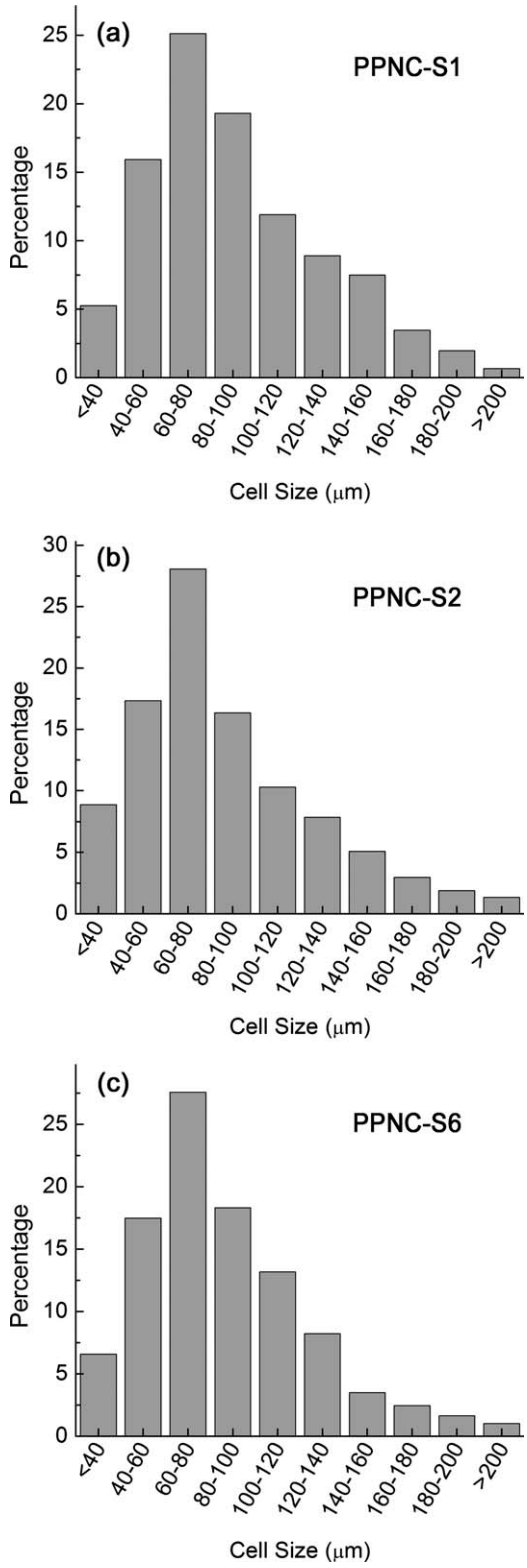

FIG. 9. Cell size distributions in extruded samples of (a) PPNC-S1 foam, (b) PPNC-S2 foam, and (c) PPNC-S6 foam.

present in the nanocomposites: high surface area, slower crystallization, and melt strain hardening in extensional flow. The higher molecular weight grade of maleated PP copolymer led to nanocomposites displaying strain hardening in melt extensional flow that is critical for producing closed-cell foams with a narrow cell-size distribution from linear PP. Further increases in melt strain hardening can be achieved by silane treatment of the organoclays used for making linear PP nanocomposites, leading to further improvement in the quality of extruded foams. This work will be presented in a subsequent paper.

CONCLUSIONS

When several PP clay nanocomposites all with good dispersion of the dialkyl amine-treated organoclay were foamed by extrusion with a chemical-blowing agent, systematic variations in foam quality were obtained based on differences among them in melt-extensional strain hardening and in crystallization behavior. Among nanocomposites that did not strain harden, a slower rate of crystallization led to closed-cell foams with smaller cell sizes and greater cell density. With nanocomposites where significant strain hardening was observed in extensional flow, the extruded PP nanocomposite foams displayed the smallest cell sizes and the greatest cell density by reducing cell coalescence. Very good foams were produced with linear PP–clay nanocomposites containing only 3 wt% of organoclay and compatibilizer chains with sufficient length to bridge the clay surfaces and cause extensional strain hardening in the melt.

ACKNOWLEDGMENTS

The authors are pleased to acknowledge a scholarship award to Amit Kumar Chaudhary from the Detroit Section of SPE and discussions on the foaming process with Dr. R. Dhavalikar of ViChem Corporation.

REFERENCES

1. C.C. Zeng, X.M. Han, L.J. Lee, K.W. Koelling, and D.L. Tomasko, *Adv. Mater.*, **15**, 1743 (2003).
2. J. Shen, C.C. Zeng, and L.J. Lee, *Polymer*, **46**, 5218 (2005).
3. M. Mitsunaga, Y. Ito, S.S. Ray, M. Okamoto, and K. Hironaka, *Macromol. Mater. Eng.*, **288**, 543 (2003).
4. Y.W. Di, S. Iannace, E. Di Maio, and L. Nicolais, *J. Polym. Sci., Part B: Polym. Phys.*, **43**, 689 (2005).
5. R. Dhavalikar, M. Yamaguchi, and M. Xanthos, *J. Polym. Sci., Part A: Polym. Chem.*, **41**, 958 (2003).
6. C. Gabriel and H. Munstedt, *J. Rheol.*, **47**, 619 (2003).
7. J. Stange and H. Munstedt, *J. Rheol.*, **50**, 907 (2006).
8. M. Okamoto, P.H. Nam, P. Maiti, T. Kotaka, T. Nakayama, M. Takada, M. Ohshima, A. Usuki, N. Hasegawa, and H. Okamoto, *Nano Lett.*, **1**, 503 (2001).
9. D. Dixon, P.J. Martin, and H.E. Jones, *J. Cell. Plast.*, **36**, 310 (2000).
10. C.H. Lee, K.J. Lee, H.G. Jeong, and S.W. Kim, *Adv. Polym. Technol.*, **19**, 97 (2000).
11. C.B. Park and L.K. Cheung, *Polym. Eng. Sci.*, **37**, 1 (1997).
12. J. Reignier, R. Gendron, and M.F. Champagne, *J. Cell. Plast.*, **43**, 459 (2007).
13. J. Stange and H. Munstedt, *J. Cell. Plast.*, **42**, 445 (2006).
14. P. Spitael and C.W. Macosko, *Polym. Eng. Sci.*, **44**, 2090 (2004).
15. J. Stange, C. Uhl, and H. Munstedt, *J. Rheol.*, **49**, 1059 (2005).
16. T.J. McCallum, M. Kontopoulou, C.B. Park, E.B. Muliawan, and S.G. Hatzikiriakos, *Polym. Eng. Sci.*, **47**, 1133 (2007).
17. S.H. Tabatabaei, P.J. Carreau, and A. Ajji, *Chem. Eng. Sci.*, **64**, 4719 (2009).
18. S.H. Tabatabaei, P.J. Carreau, and A. Ajji, *Polym. Eng. Sci.*, **50**, 191 (2010).
19. C. Liu, D. Wei, A. Zheng, Y. Li, and H. Xiao, *J. Appl. Polym. Sci.*, **101**, 4114 (2006).
20. D.H. Han, J.H. Jang, H.Y. Kim, B.N. Kim, and B.Y. Shin, *Polym. Eng. Sci.*, **46**, 431 (2006).
21. M. Danaei, N. Sheikh, and F.A. Taromi, *J. Cell. Plast.*, **41**, 551 (2005).
22. F. Yoshii, T. Sasaki, K. Makuuchi, and N. Tamura, *J. Appl. Polym. Sci.*, **31**, 1343 (1986).
23. A. Yousefi and A.A. Katbab, *Radiat. Phys. Chem.*, **44**, 645 (1994).
24. L.J. Lee, C.C. Zeng, X. Cao, X.M. Han, J. Shen, and G.J. Xu, *Compos. Sci. Technol.*, **65**, 2344 (2005).
25. M. Guo, M. Heuzey, and P.J. Carreau, *Polym. Eng. Sci.*, **47**, 1070 (2007).
26. W.G. Zheng, Y.H. Lee, and C.B. Park, *J. Appl. Polym. Sci.*, **117**, 2972 (2010).
27. M. Antunes, J.I. Velasco, V. Realinho, and E. Solorzano, *Polym. Eng. Sci.*, **49**, 2400 (2009).
28. M.F. Champagne and R. Gendron, *Soc. Plast. Eng. Tech. Pap.*, **51**, 1477 (2005).
29. M. Okamoto, P.H. Nam, P. Maiti, T. Kotaka, N. Hasegawa, and A. Usuki, *Nano Lett.*, **1**, 295 (2001).
30. T. Pathak and K. Jayaraman, *Soc. Plast. Eng. Tech. Pap.*, **53**, 133 (2007).
31. H.E. Naguib and C.B. Park, *Polym. Eng. Sci.*, **42**, 1481 (2002).
32. J.W.S. Lee, K.Y. Wang, and C.B. Park, *Ind. Eng. Chem. Res.*, **44**, 92 (2005).
33. W. Kaewmesri, P.C. Lee, C.B. Park, and J. Pumchusak, *J. Cell. Plast.*, **42**, 405 (2006).
34. H.E. Naguib, C.B. Park, and N. Reichelt, *J. Appl. Polym. Sci.*, **91**, 2661 (2004).
35. H. Munstedt, S. Kurzbeck, and J. Stange, *Polym. Eng. Sci.*, **46**, 1190 (2006).
36. N. Katsikis, T. Koniger, and H. Munstedt, *Appl. Rheol.*, **17**, 52751 (2007).
37. M. Yamaguchi, *J. Polym. Sci., Part B: Polym. Phys.*, **39**, 228 (2001).
38. A. Somwangthanaroj, E.C. Lee, and M.J. Solomon, *Macromolecules*, **36**, 2333 (2003).

 DOI 10.1002/pen